Dynamics of Agulhas Retroflection and Ring Formation in a Numerical Model. Part II. Energetics and Ring Formation

ERIC P. CHASSIGNET AND DOUGLAS B. BOUDRA

Rosenstiel School of Marine and Atmospheric Science, University of Miami, Miami, Florida

(Manuscript received 30 December 1986, in final form 11 September 1987)

ABSTRACT

An energetics analysis of several numerical experiments on an idealized South Atlantic–Indian Ocean basin is presented. The model used in the experiments is the quasi-isopycnic coordinate model of Bleck and Boudra forced by wind and configured with two or three layers. The region of focus is the most dynamically active one, the Agulhas Current retroflection south of Africa, and the dynamical mechanisms associated with formation of Agulhas rings are given special attention.

Whether rings form in the model and their frequency depend on two primary factors: the shape of Africa and southward inertia/baroclinicity in the overshooting Agulhas. The boundary condition on Africa (no-slip/free-slip) and horizontal resolution are also important. Experiments in which rings form exhibit considerably larger values of K_M to K_E transfer than those in which no rings form. In three of the experiments, ring formation is studied in detail with the help of instantaneous top and bottom layer flow patterns and time series energetics. In a low Rossby number experiment with a rectangular Africa, rings are formed almost continuously, and basin mode resonance plays a significant role in ring formation. Whether a form of instability (barotropic or baroclinic) plays an important role as well is unclear. In two high Rossby number experiments, one with rectangular and the other with triangular African geometry, basin mode resonance is not a factor, and, it is suggested that ring formation is associated with release of mixed barotropic–baroclinic instability.

1. Introduction

The channel surrounding Antarctica is the major link connecting the different oceans, and thus, most previous Southern Ocean research has concentrated on the Antarctic Circumpolar Current. However, the large distance between South Africa and Antarctica provides an opportunity for direct exchange between the subtropical gyres of the Indian and Atlantic Oceans. The Agulhas Current constitutes the South Indian Ocean's primary western boundary current and the major part of it retroflects south of the tip of Africa, returning eastward to the Indian Ocean. On the coastal edge of the current, however, Indian Ocean water leaks around the Cape of Good Hope. Also, several times a year, in retroflecting, the Agulhas doubles back and cuts itself off. Lenses of warm, salty Indian Ocean water, formed in this fashion (hereafter referred to as Agulhas rings), translate into the Atlantic, providing an additional influx of Indian Ocean water. Estimates from field measurements suggest tranfer rates of Indian Ocean water into the Atlantic from 5×10^6 m^3 s^{-1} (Harris et al., 1978) to 14×10^6 m^3 s^{-1} (Gordon, 1985). This Indian Ocean water is considerably warmer than that in the eastern subtropical South Atlantic, and such an input of heat into the Atlantic might be related to the abnormal northward ocean heat flux across 30°S in the Atlantic, pointed out, among others, by Stommel (1980). In addition, a recently developed controversial theory by Gordon (1986) suggests the importance of such a transfer in the global interocean exchange of thermocline water.

Historically, Agulhas rings have been described by only a few authors (Duncan, 1968; Harris et al., 1978; Lutjeharms and Gordon, 1987). Recently, Olson and Evans (1986) suggested that Agulhas rings are several times more energetic than other large rings in the world ocean, such as Gulf Stream rings in the area around the New England Seamounts or Gulf of Mexico Loop Current rings. Several ring formation events were described by Lutjeharms (1981) and Lutjeharms and Gordon (1987) with the help of thermal infrared satellite imagery. In addition, an investigation of four years of daily satellite images by Lutjeharms and van Ballegooyen (1987) suggests that rings are shed at intervals of 1.5–2 months. But little has been established about the dynamics that drive the shedding and frequency, mostly because the rings are strongly nonlinear features. For example, might the formation of the rings and the associated leakage be strongly influenced by seasonal factors (wind stress or inflow) or by nonlinear oscillations of the recirculation region off South Africa? There seems to be no strong evidence supporting either notion. Observational efforts to find time-dependence in

Corresponding author address: Dr. Douglas B. Boudra, Rosenstiel School of Marine & Atmospheric Science, 4600 Rickenbacker Causeway, Miami, FL 33149-1098.

the Agulhas Current transport by Pearce and Gründlingh (1982) were not conclusive. Also, in their numerical study of a related phenomenon, the dynamics of loop current eddy shedding in the Gulf of Mexico, Hulburt and Thompson (1980) obtained a quasi-annual eddy shedding without any fluctuating forcing. Even with realistic time variation of the upper-layer inflow, the eddy-shedding period was dominated by the quasi-annual period rather than by the forcing period, although the influence of the latter was not negligible.

In this paper, the Agulhas retroflection region in an idealized model of the wind-driven South Atlantic–Indian Ocean circulation is analyzed in detail. In Part I (Boudra and Chassignet, 1988; hereafter referred to as BC), focus is on the retroflection vorticity balance. Here in Part II, we study the energetics of the retroflection and the ring formation process. The eddy-mean energetics of a number of experiments are examined in order to gain additional understanding of the model retroflection. It is shown that as the mean upper layer thickness is decreased, the boundary currents develop more vertical shear. This leads to more strongly tilted isopycnal surfaces and to more energy exchange between the mean kinetic energy (K_M) and the available potential energy (P). With this increase in vertical shear, the boundary currents' inertia increases, more fluid retroflects and fewer rings are formed. In contrast, experiments in which ring formation is regular are more dominated by energy exchange between K_M and the eddy kinetic energy (K_E). In three of the experiments, the signatures of barotropic and baroclinic instability in ring formation are also examined in some detail. In a relatively low Rossby number experiment, rings are formed almost continuously, and basin mode resonance plays a significant role in ring formation. Whether a particular instability is strongly tied to ring formation is not clear. In two highly nonlinear experiments, the basin mode resonance is only weakly evident, and each exhibits a maximum in the conversion terms $C(K_M, K_E)$ and $C(P, K_E)$ near ring cutoff. Simultaneously, bottom layer features underneath the retroflection greatly intensify, characteristic of release of baroclinic instability. The latter is confirmed by a decrease (increase) in basin-averaged potential energy (kinetic energy). It is therefore suggested that, in these experiments, ring formation is associated with release of mixed barotropic-baroclinic instability.

In section 2, we review the model characteristics and provide a table of the experiments. The formulation of the energy conversion terms is presented in section 3. The time averaged eddy-mean energetics is investigated in section 4 for seven numerical experiments. In section 5, we first illustrate some characteristic features of the ring formation process in three of the experiments, using instantaneous flow patterns of the top and bottom layers. We then investigate the instabilities associated with ring formation using curves of domain-averaged energies and energy conversions versus time. We summarize the results of our analysis in section 6. In the concluding section we compare with several other modeling studies and discuss the limitations of the model.

2. Description of the model and the experiments

The model used in this study is a primitive equation quasi-isopycnic coordinate model developed by Bleck and Boudra (1981). In a set of ten multilayer experiments, the model was used to study the wind-driven circulation of the South Atlantic–Indian Ocean, especially as influenced by the strength of the Agulhas retroflection, in Boudra and de Ruijter (1986, hereafter referred to as BD). Since fluid is exchanged between layers very rarely in these experiments, the model is effectively a "purely" isopycnic coordinate one in this study. The parameters and the character of retroflection and ring formation for the experiments are presented here in Table 1, which also indicates where more complete descriptions have been given. The basins used are illustrated in Fig.1. The idealized basin is rectangular with a grid spacing of either 20 or 40 km. Africa is represented by either a rectangle, extending halfway into the basin, or a triangular, more realistic shape, taking into account the orientation of the Agulhas Bank. In the latter configuration (Experiment E11 only), the planetary vorticity advection in the separating Agulhas, felt to be important in the strength of the retroflection, is given more realistic importance. The crosses in the figure indicate where special calculations are made for later discussion.

The circulation in the model is driven by a steady wind stress of which the profile is shown at the left of Fig. 1. The wind curl vanishes 400 km south of the tip of Africa. The conditions on meridional boundaries are generally no-slip ($u = v = 0$) and those for zonal boundaries free-slip ($v = du/dy = 0$), except in one experiment where the coast of Africa is treated homogeneously as a free-slip boundary. The resulting circulation pattern includes anticyclonic subtropical gyres in the Atlantic and Indian sectors, respectively, and an elongated cyclonic subpolar gyre south of the wind curl zero. The degree of interaction between the two subtropical gyres is determined by the strength of the Agulhas retroflection. For further details on the experiments, the reader is referred to BD and BC.

3. Formulation of the energetics

The basin-averaged mean and eddy kinetic energies are expressed as

$$K_M = \frac{1}{gA}\int_A \int_{\text{bot}}^{\text{top}} \left(\frac{\tilde{v}^2}{2}\right)\frac{\overline{\partial p}}{\partial s}\, dsdA, \qquad (3.1)$$

the kinetic energy associated with the mean flow, and

TABLE 1. Description of the experiments. Blanks indicate no change from the previous experiment.

Experiment	Number of layers	Thickness of the layers (m)	g' ($m\ s^{-2}$)	Viscosity ($m^2\ s^{-1}$)	Bottom drag coefficient (s^{-1})	Boundary conditions on Africa[1]	Horizontal resolution (km)	Africa's geometry[1]	Characteristics of layer one exchange between Indian and Atlantic (where previously described)
E1	2	1 000 4 000	0.02	330	0	NS	40	A	Total of 25 Sv exchange, including about 4 rings per year. (Boudra and de Ruijter, 1986) (BD) and (Boudra and Chassignet, 1988) (BC).
E2	3	600 700 3 700	0.02 0.005						Total of 15 Sv exchange, including 3 to 4 rings per year. (BD and BC).
E3		300 900 3 800							No rings, less than 5 Sv leakage. (BD and BC).
E8					10^{-7}				Same as E3. (BD and BC).
E9						FS			Most of the flow turns westward and then northward around the tip of Africa into the Atlantic and returns in the free jet to the south. (BD and BC).
E10						NS	20		Less than 5 Sv exchange. Four rings in 10 years. (BD and BC).
E11								B	Mean exchange of 5 Sv, including about 3 rings/year. (BC)

[1] NS = No-Slip, FS = Free-Slip.
[2] A = Rectangular, B = Triangular.

$$K_E = \frac{1}{gA}\int_A \int_{\text{bot}}^{\text{top}} \overline{\left(\frac{v'^2}{2}\right)\frac{\partial p}{\partial s}}\, ds dA, \tag{3.2}$$

the kinetic energy associated with the transient eddy field, where s is the generalized vertical coordinate, density here; $(\bar{\ })$ is the time average; $(\tilde{\ })$ is the mass weighted time average; $(\ )'$ the departure from the mass weighted time average; A is the total basin area and the other symbols are conventional. The available potential energy associated with each layer interface k is expressed as

$$P_k = \frac{1}{gA}\int_A \frac{1}{2}(p_k - \hat{p}_k)^2 \Delta\rho_k dA \tag{3.3}$$

where $\hat{p}_k$ is the basin-averaged pressure on the kth interface, and $\Delta\rho_k$ is the density change across that interface. To compute the total available potential energy, (3.3) is summed over the internal interfaces. Bleck and Boudra (1981) have shown that the upper surface potential energy is approximately three orders of magnitude smaller than that associated with the internal interfaces, and its contribution is neglected here.

The form of energy conversion terms using isopycnic vertical coordinates has been derived by Bleck (1985) and used by Bleck and Boudra (1986) in an eddy-resolving intercomparison of pure isopycnic, quasi-isopycnic and isobaric coordinate models. In the latter paper, because of 1) a conflict between the isopycnic and isobaric coordinate definitions of eddy potential energy and 2) differences between some of the conversion terms in conventional analysis and in isopycnic coordinates, potential energy was not split into mean and eddy components, and the same is true here.

Following the generalized coordinate notation used by Bleck (1985), the conversion terms are as follows:

$$C(P, K_E) = \overline{\phi\nabla_s\cdot\left(\frac{\partial p}{\partial s}v'\right)} - \overline{v'\cdot\frac{\partial p}{\partial s}\alpha\nabla p}$$

$$C(P, K_M) = \overline{\phi\nabla_s\cdot\left(\frac{\partial p}{\partial s}\hat{v}\right)} - \hat{v}\cdot\overline{\frac{\partial p}{\partial s}\alpha\nabla p}$$

$$C(K_M, K_E) = -\overline{v'\frac{\partial p}{\partial s}\cdot\left(v'\cdot\nabla_s + s'\frac{\partial}{\partial s}\right)\tilde{v}} \tag{3.4}$$

where ϕ is the geopotential, $C(P, K_E)$ represents the buoyancy work (i.e., baroclinic conversion) and $C(K_M, K_E)$ represents the transfer of energy from the mean to the disturbance flow, or vice versa, through the Reynolds stress interacting with the shear of the mean flow (i.e., barotropic conversion) (Dutton, 1973).

4. Eddy-mean energetics

In order to gain some additional insight into the impact of the model parameters most influential on the retroflection, we now examine the eddy-mean energetics of the experiments listed in Table 1, illus-

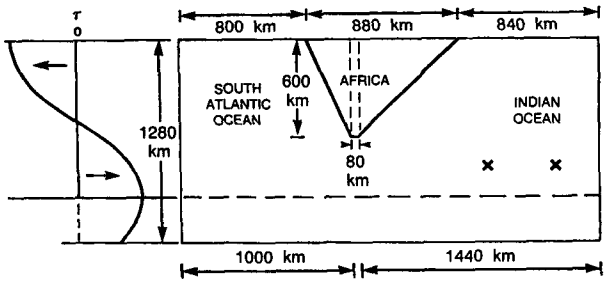

FIG. 1. Geometry of the flat bottom basin used in all experiments. The wind stress profile is shown at the left. The crosses indicate the locations where kinetic energy spectra are computed for E1 and displayed in Fig. 4.

trated in box diagram form in Fig. 2. The time means of the energies and conversion terms of the experiments in the final, statistically steady state, averaged over the model domain, are computed over the last five years of a ten year run for E1, E2, E3, E8, E9 and E11 and over selected years for E10. We use the term "year" only to represent a 365 day period since the wind forcing is held constant.

The first series of experiments, E1–E3, varies the depth of the top layer—the one which receives most of the direct wind forcing—and primarily illustrates the influence of the boundary current inertia and baroclinicity on the two ocean circulation. The top layer is 40% thinner in E2 than in E1 and the number of layers increases from two to three. The top layer is still thick enough, however, that virtually all the Sverdrup transport is trapped in it. Therefore, its overall flowspeed increases, and this increase has its greatest impact in the western boundary currents, where the velocities are already relatively large. Through geostrophic adjustment, this leads to a more sharply inclined isopycnal interface between layers 1 and 2, and, thus, to an increase in available potential energy. But K_M increases only slightly from E1 to E2 (Fig. 2a, b). This difference may be viewed in terms of the portion of the potential and kinetic energies associated with the vertical mean and shear flows. The potential energy associated with the vertical mean flow is the sea surface available potential energy, which is orders of magnitude smaller than the layer interface potential energies, as pointed out in section 3. Changes in P, therefore, should be strongly linked with changes in vertical shear, and the accompanying changes in isopycnal inclination. On the other hand, kinetic energy is positively correlated with increases in vertical shear only in that the latter brings about larger velocities in some portion of the column. From (3.1), it is seen that the contribution to K_M of the square of the velocity from each layer is weighted by the layer thickness, $\partial p/\partial s$. Considering the difference of E2 from E1, the top layer velocities are larger in the former, but a greater thickness of fluid has weak motion. Thus, as the baroclinicity increases, the K_M associated with the vertical mean flow decreases, while that associated with the vertically sheared flow increases, and the total remains about the same. The increase in boundary current inertia through thinning of the top layer depth, therefore, has a much larger impact on the potential energy than on the kinetic energy. Rings are continuously being formed in the Agulhas retroflection region in both experiments and the increase in strength and baroclinicity of the boundary currents from E1 to E2 results in more instability and more $C(P, K_E)$ and $C(K_M, K_E)$.

The top layer is 50% thinner in E3 (Fig. 2c) than E2, so that the boundary currents are even more inertial and vertically sheared. A major difference from E1 and E2, however, is that the subtropical circulations in the Indian and Atlantic oceans are almost isolated from each other. As shown in BD, this leads to a dramatic increase in available potential energy, especially in the Indian Ocean portion of the basin. The baroclinicity in the boundary currents continues to increase, but no Agulhas rings are formed, apparently accounting for the reduction in $C(K_M, K_E)$, even though there is substantially more K_E in E3. The conversion through the other path from K_M to K_E—that is, through P—more than doubles in magnitude from E2 to E3 because of the increased baroclinicity.

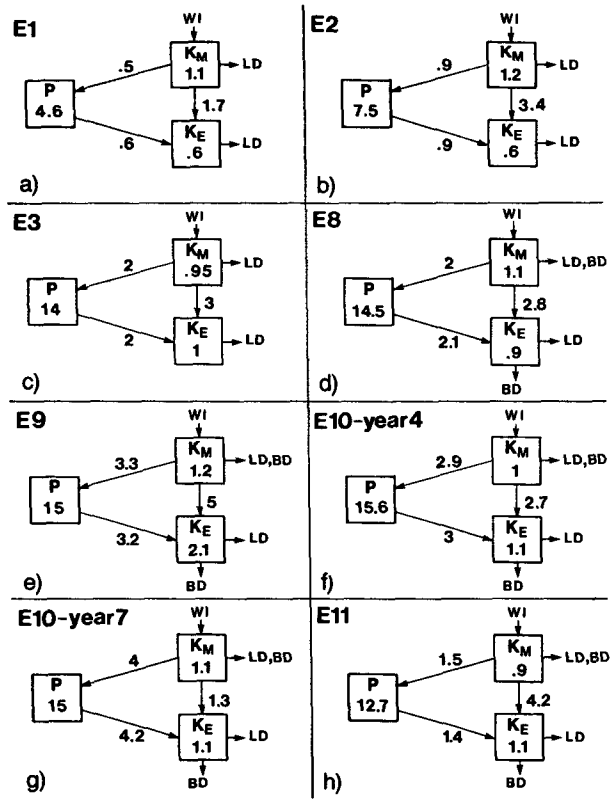

FIG. 2. Basin average eddy-mean energetics for (a) E1; (b) E2; (c) E3; (d) E8; (e) E9; (f) E10, year 4; (g) E10, year 7; (h) E11. WI is the wind input; LD, the lateral dissipation and BD, the bottom drag. P, K_M and K_E are in 10^4 J m^{-2} and the conversion terms in 10^{-2} W m^{-2}.

Inclusion of bottom drag in E8 (Fig. 2d) reduces the bottom layer circulation intensity. This leads to a more stable and intense retroflection in the top layer because the more variable bottom layer flow regime in E3 is a primary mechanism for draining energy westward from the retroflection area. Therefore, there is slightly more K_M and less K_E in E8, but the conversions are largely as in E3.

In the free-slip Africa case E9 (Fig. 2e), otherwise similar to E8, where most of the fluid goes around the southern tip of Africa into the Atlantic, the total kinetic energy is 50% higher than in E8, primarily because of the reduction of kinetic energy dissipation along the coast of Africa. The boundary currents and the free jet in the South Atlantic become stronger, and through geostrophic adjustment, P and the exchange between kinetic and potential energies increase also. As pointed out by BC, the flow regime is particularly turbulent south of Africa in this experiment, leading to large values of K_E and $C(K_M, K_E)$.

In E10, grid-point spacing is halved to 20 km. Otherwise, the parameters are as in E8. Increases are noticed in P and in the potential to kinetic energy conversions because the boundary currents are more strongly sheared than in E3 and E8, and because their instability is more easily released with this finer resolution, respectively. Since four rings were formed during the ten year experiment, it is also interesting to note the difference in the energetics for years without and with ring formation. In the latter case, the baroclinic and barotropic transfers are about the same magnitude (Fig. 2f). During a year without a ring, the $K_M \rightarrow P \rightarrow K_E$ transfer appears to be the primary energy path (Fig. 2g). This comparison strongly suggests the association between $C(K_M, K_E)$ and the ring formation process.

Further supporting this relationship is the fact that the change in South Africa's geometry results in more barotropic conversion. In fact, the dominant transfer is the one from K_M to K_E (Fig. 2h). A major difference between the two experiments is the much greater number of rings formed in E11, the primary mechanism by which Indian Ocean water leaks into the Atlantic in the experiment. Also, P is approximately 15% smaller in E11 than in E10 because the retroflection is less intense and the Agulhas along the boundary is somewhat broader.

5. Ring formation

In this section, we investigate the model Agulhas ring formation process by examining events in three of the above experiments, using both instantaneous flow patterns of top and bottom layers and curves of domain-averaged energies and energy conversions versus time. As can be seen from Table 1, the character and frequency of ring formation depend on the choice of parameters. Boudra and Chassignet (1988) develop the physical explanation for the strength of the retroflection, which is strongly related to the frequency of ring formation. As the Rossby number/baroclinicity of the boundary currents is increased through thinning the top layer, more fluid retroflects and fewer rings are formed. With 40 km grid resolution, rings are formed in the low Rossby number cases (E1 and E2), but not in the high Rossby number cases (E3 and E8). On the other hand, an experiment not illustrated here, with the E11 African geometry but otherwise similar to E8, exhibited two to three ring formation events per year. With the rectangular African geometry, a few rings also form as grid spacing is halved (E10), better resolving the release of baroclinic instability. In order to gain some understanding of ring formation in our model experiments, we first describe that in the relatively low Rossby number, two-layer experiment E1 and then that in the higher resolution experiments E10 and E11 (Δx = 20 km). The last subsection (d) focuses on ring formation as a possible current instability, using time series energetics and a discussion of the horizontal and vertical structure of the events presented in subsections a, b and c.

a. Flow characteristics of E1 (low Rossby number, rectangular Africa)

Rings are formed in E1 in an almost continuous manner at the southern tip of Africa at a rate of about four per year. In most cases, as soon as a previously formed ring begins to drift toward the Atlantic, the center of the retroflection moves southward and, shortly thereafter, a new ring begins to form. The regular ring formation in this experiment is accompanied by a continual leakage of Indian Ocean water around the tip of Africa.

A typical event of E1 is illustrated in Fig. 3 starting at day 3050. An already formed ring is moving westward and is being absorbed by the Atlantic subtropical gyre. The main Agulhas overshoots Africa and turns eastward into the Indian Ocean. The instantaneous flow pattern includes top and bottom layer anticyclonic eddies at the southern tip of Africa (Fig. 3a, b). From day 3050 to day 3070, the intensity of the retroflection eddy increases as it is fed with Agulhas water, and the bottom layer eddy underneath it intensifies, as energy is transferred downward (Fig. 3c, d, e, f). Simultaneously, the bottom layer eddy exhibits steady westward movement and the top layer retroflection eddy follows closely, as if to minimize the development of vertical shear. Around day 3080, the top layer eddy detaches from the Indian subtropical gyre, forming a ring (Fig. 3g). In the bottom layer, the anticyclonic eddy is still moving westward, leading the top layer ring (Fig. 3j). The ring then moves in a west-northwestward direction until it gets absorbed into the Atlantic subtropical gyre.

A characteristic of E1 which may be related to ring formation at Africa's tip is the organized structure of

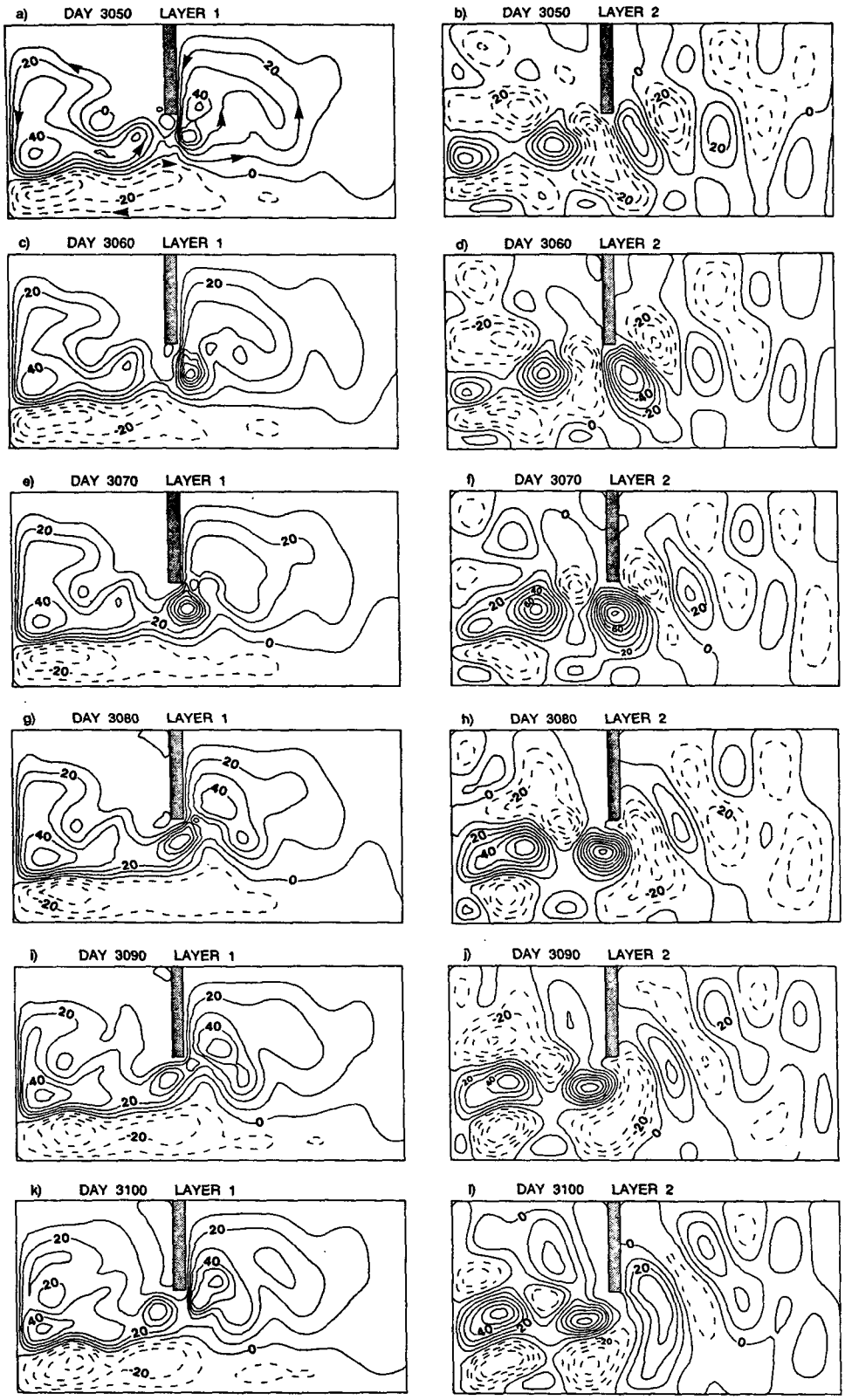

FIG. 3. Top and bottom layer mass transport streamfunctions for a ring formation event in E1. The contour interval is 10 Sv.

elongated eddies in the bottom layer propagating east to west (Fig. 3b, d, f, h, j, l). Such a structure is representative of basin-mode resonance (Longuet-Higgins, 1964) and is found in many eddy-resolving general circulation models (Miller et al., 1987). An inspection of kinetic energy spectra at various locations will help us to identify the signatures of these basin modes, as shown by the latter authors for Experiment 1 of Holland (1978). A regular passage of eddies in the bottom layer is found in E1 at locations (x = 1880 km, y = 480 km) and (x = 2280 km, y = 480 km), denoted by the crosses in Fig. 1, at a period of approximately 60 days. The cyclonic and anticyclonic phases of these eddies each contribute equally to the kinetic energy spectra with a period of 30 days (Fig. 4). According to Longuet-Higgins (1964), the period T for the barotropic mode (m, n) in a rectangular basin $a \times b$ is equal to

$$T = \frac{4\pi}{\beta}\left(\frac{m^2\pi^2}{a^2} + \frac{n^2\pi^2}{b^2}\right)^{1/2}. \qquad (5.1)$$

The mode (5, 2) is the one suggested by the configuration of the bottom layer eddies and is the most likely to appear because of the position and length of Africa with respect to the basin dimensions. The rectangular Africa constitutes a nodal line and its position, located a distance $^2/_5$th of the width of the basin from the west side, favors the development of the wavenumber 5 in the east–west direction. In the north–south direction, the wavenumber 2 develops since Africa extends about halfway into the basin. The corresponding period from (5.1) is $T \sim 60$ days, in agreement with the above findings.

As mentioned above, after the formation of a ring, as the top layer recirculation eddy reestablishes at the tip of Africa, an anticyclonic eddy intensifies in the bottom layer and shows steady westward progress. This displacement is not always accompanied by the formation of a ring. However, each time a ring is formed, an anticyclonic circulation in the bottom layer leads its westward propagation. The period corresponding to the motion of this particular bottom layer eddy is also 60 days and, as a consequence, intervals between ring formation events are multiples of this period (usually 1 or 2).

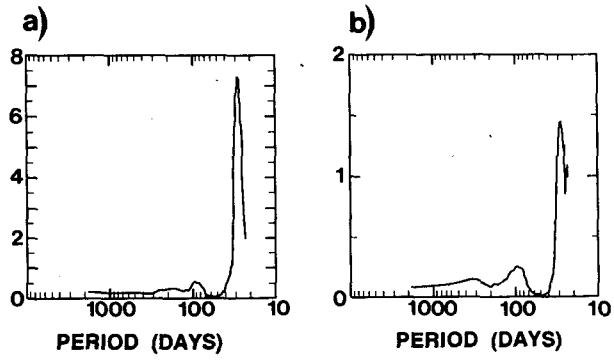

FIG. 4. Variance conserving spectra of the bottom layer kinetic energy in E1 at the locations shown in Fig. 1, (a) x = 1880 km, y = 480 km; (b) x = 2280 km, y = 480 km. Units are in 10^6 J^2 m^{-4}.

The question then arises as to whether basin modes are important in determining the eddy shedding period or if they are simply generated and maintained by the ring formation dynamics. Ring generation at the southern tip of Africa, because it is associated with large fluctuations in the top layer mass and flow fields, is a source of energy for bottom layer features. Miller et al. (1987) state that resonantly excited basin modes are driven by localized instabilities and feed on the turbulence. Factors that limit the resonant response of these modes in the far field are friction and nonlinearities (Pedlosky, 1965).

To gain some insight into the relationship between basin modes and ring formation, we have run two experiments with linear bottom drag, otherwise similar to E1. Space is limited here and there is no need to give a full description of these experiments. But their essential character with respect to ring formation and basin modes is of relevance to our discussion. In the first experiment, with a relatively strong drag (10^{-7} s^{-1}), much of the upper layer energy in the retroflection area is transfered downward and dissipated through bottom friction, leaving most of the rings formed very weak. In the second experiment, with a drag half as large as the previous one (5×10^{-8} s^{-1}), rings are as strong as in E1 most of the time, but are also very weak in a few cases.

In these two experiments, the kinetic energy spectra show an effective damping of the basin modes (one to two orders of magnitude) and the bottom layer features east of the retroflection region are now very weak. However, the ring formation process remains as in E1. In the three experiments, as the recirculation eddy in the top layer builds up at the tip of Africa, energy from it is transferred downward into the bottom layer and energizes the basin modes. The frequency of these basin modes and their propagation speed are unaffected by the damping. The propagation speed after separation of both the ring and the bottom layer anticyclone is approximately 10 cm s^{-1} which corresponds to the 60 day period of the basin modes and is considerably faster than the propagation of isolated eddies in ocean models, which, as Nof (1983) points out, is usually of the order of the long Rossby wave speed, 3.2 cm s^{-1}, defined by βR_d^2.

In E1 and the two subsidiary experiments with bottom drag, the events leading up to ring formation are controlled by the larger scale dynamics in the top layer (reestablishment of the retroflection eddy after a ring has been formed and then drifted westward). But the actual frequency of ring cutoff and the ring's subsequent westward motion are strongly related to those of the bottom layer features (representation of the basin mode resonances), suggesting an important dynamical connection between them. The top layer eddy breaks free

from the retroflecting Agulhas with the westward motion of the bottom layer anticyclone underneath it. In this low Rossby number case, then, the tendency to maintain a vertically coherent structure overwhelms that for the upper layer eddy to be locked within the retroflection by the Agulhas.

b. Flow characteristics of E10 (fine resolution, high Rossby number, rectangular Africa)

The formation process is quite different in E10, where only four rings form during ten years. Basin mode-type bottom layer features with a period of 45 days are present in this experiment, but are energetically significant only in the extreme eastern part of the basin. The increase in nonlinearity, resolution, and number of layers, as well as inclusion of bottom drag, effectively decrease their magnitude and influence on ring formation. The strong nonlinearity of this experiment leads to a leakage around the tip of Africa of less than 5 Sv (1 Sv $\equiv 10^6$ m^3 s^{-1}) (see BD, BC). Rings form southeast of the tip of Africa, contrary to the above, weakly nonlinear E1 where they form southwest of it. For a ring to cut off in E10, the center of the retroflection must be rather far south, and a large volume of fluid from the subpolar gyre must intrude northward along the east side of the retroflection region. Such an event occurs at the end of year 8. The ring is first formed near day 2890, then reattaches to the subtropical Indian gyre, but retains its identity as an eddy. The final cut off of the ring occurs near day 2935. The latter stages of this ring shedding and its subsequent westward and northwestward motion were previously illustrated by BD.

The initial ring formation is illustrated in Fig.5 starting at day 2875. Five days later, the cyclonic meander just east of the retroflection eddy has begun to amplify and fluid from the subpolar gyre is moving northward within it (Fig. 5c). In the bottom layer (Fig. 5d), an anticyclonic eddy underneath the retroflection intensifies. In addition, a cyclonic circulation in the vicinity of the intrusion of subpolar water extends westward and is associated with the cyclonic member of a strong dipole in the northwestern part of the Indian sector. By day 2885, as energy is pumped into the bottom layer, the cyclonic circulation there intensifies and reaches the African coast (Fig. 5f). The top layer recirculation eddy at the tip of Africa is draining fluid from the subpolar gyre along its eastern side and a cyclonic circulation starts to develop within the meander (Fig. 5e). During the next five days, a vortex–vortex interaction (Lamb, 1932) between the recirculation eddy and this cyclonic circulation, now cut off from the meander, results in ring formation (Fig. 5g). In the bottom layer (Fig. 5h), by day 2890, the cyclonic circulation has become less intense and the anticyclonic eddy has begun moving westward, leading the top layer ring.

During the next 10 days, however, the coastal Agulhas returns southward and reabsorbs the ring before it can propagate significantly westward. The ring remains weakly attached to the retroflecting current until about day 2935 when it finally escapes (Fig. 6). In the final cutoff, the conditions under which the ring escapes are 1) intrusion of a large amount of water from the subpolar gyre along the east and northeast side of the recirculation eddy, effectively isolating it from the main Agulhas, and 2) a position for the subpolar front far enough south that an easy westward exit is possible. Associated with this cutoff, there is no intensification of the bottom layer eddy field under the retroflection. The propagation speed after separation is approximately 4 cm s^{-1}, considerably smaller than in E1, where it was dictated by that of the basin modes.

c. Flow characteristics of E11 (high Rossby number, fine resolution, triangular Africa)

Rings in E11 are formed along the coast (South Africa/Agulhas Bank), contrary to the rectangular Africa cases where the rings form south of the tip. Two to three rings are formed per year. As in E10, basin mode resonance is present (50 day period) but can only be discerned in the extreme eastern part of the basin.

A typical event of E11 is illustrated here in Fig. 7. In the top layer, at day 2950 (Fig. 7a), the flow pattern is in a quasi-steady configuration. An already formed ring is centered just southeast of the tip of Africa and the retroflection of the Agulhas proper is a short distance up the coast. Thirty days later, the meander east of the retroflection has begun to amplify and the center of the retroflection is moving southwest (Fig. 7c). The previously formed ring has begun moving toward the Atlantic. The bottom layer flow pattern at day 2950 shows a couplet of cyclonic eddies, one of which is under the meander (Fig. 7b). As the amplitude of the top layer meander grows, the two cyclonic eddies merge and intensify (Fig. 7d, f). Simultaneously, as energy is transferred downward, the bottom layer anticyclone located underneath the retroflection intensifies. In addition, in the top layer, a weak cyclonic circulation is generated in the meander and the future ring is drawing more and more fluid northward along its eastern side until cutoff. It is at this point (Fig. 7g), just before the cutoff, that the top layer flow pattern most resembles the flow configuration in the Ou and de Ruijter (1986) model, when the current loops back to intercept itself, although it is also here that their model breaks down. A bottom layer anticyclonic eddy leads the propagation of the already formed ring and the one referred to above leads the southwestward movement of the retroflection. The bottom layer cyclone reaches maximum intensity when the ring cuts off (Fig. 7h) and weakens rapidly thereafter (Fig. 7j). The propagation speed of the already formed ring after rounding the southern tip of Africa is approximately 5 cm s^{-1}. Interaction of the ring with the boundary may be important in this ex-

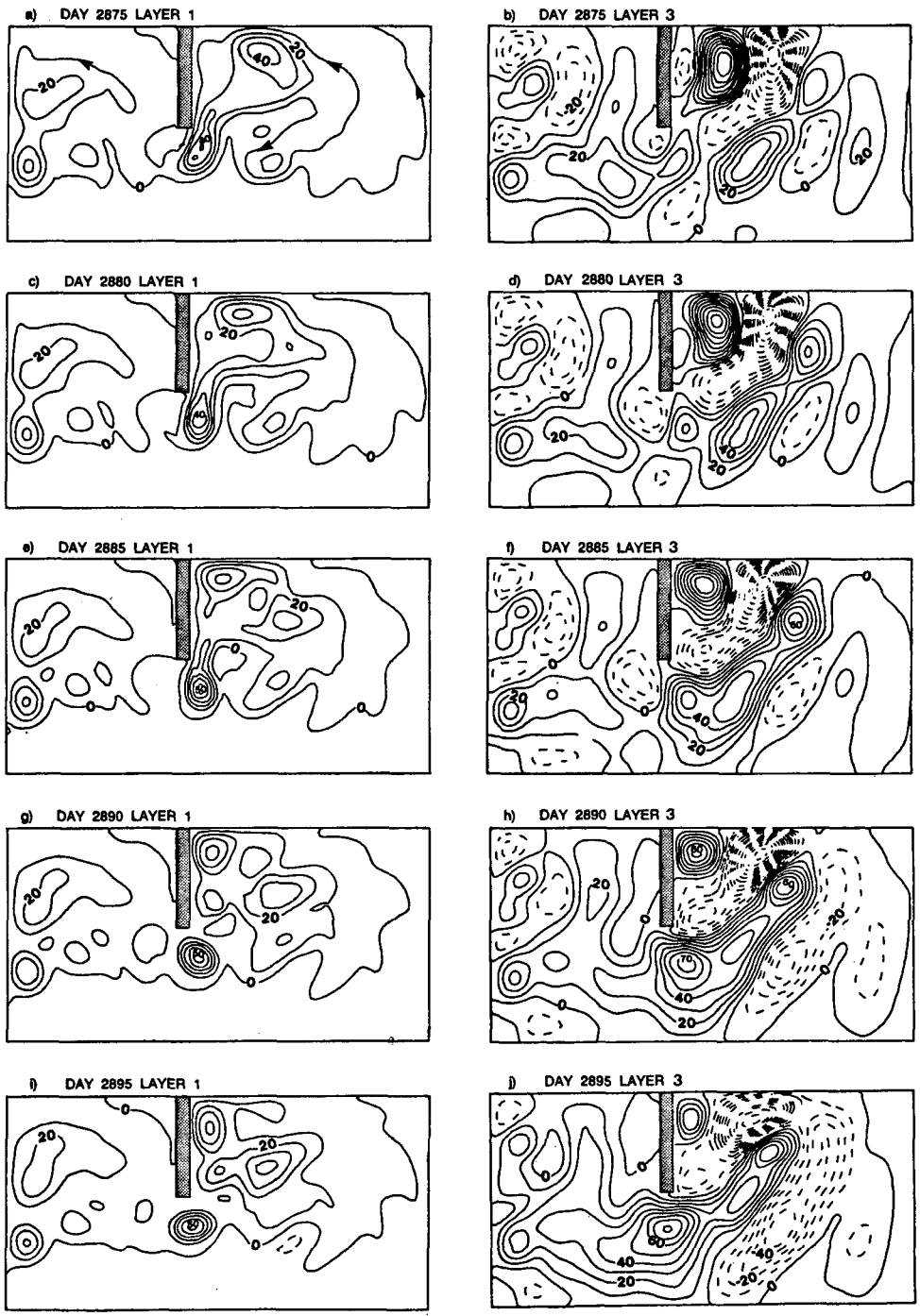

FIG. 5. As in Fig. 3 for E10 (day 2875–2895).

periment and is currently being investigated as part of a separate study focused on isolated eddy motion and behavior, using the same numerical model.

d. Discussion of the ring formation as a current instability

One might undertake a stability analysis to determine instability mechanisms, unstable wavelengths, and growth rates involved in our model ring formation, but the configuration of the current would likely be troublesome. Short of rigorous stability analysis and in order to obtain more insight into the dynamics of ring formation, we may examine the time evolution of the energies and energy conversion terms during ring formation in the three experiments discussed above.

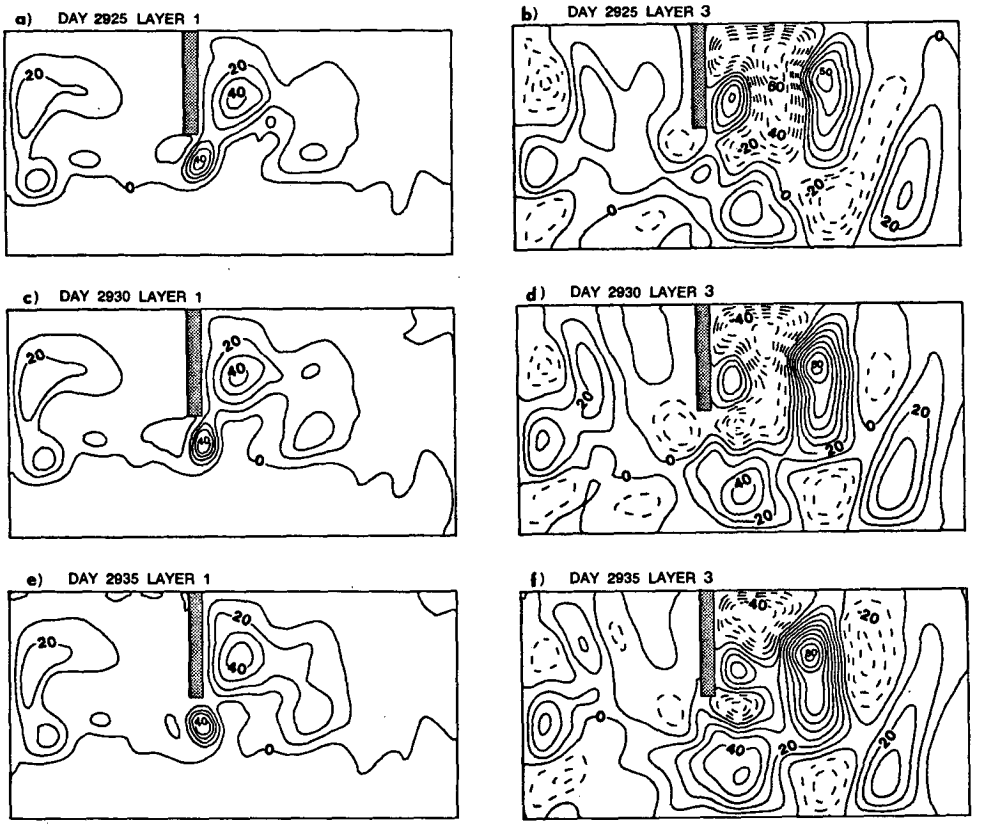

FIG. 6. As in Fig. 3 for E10 (day 2925–2935).

The mean components in the energetics are computed as averages over time (two years for E1 and one year for E10 and E11), and we investigate the growth of perturbations around this basic state. It must be kept in mind that $C(K_M, K_E)$ and $C(P, K_E)$ are associated with transfer to or away from a fluctuation flow field and it is not clear that they are directly related to barotropic and baroclinic instabilities, respectively. Peaks in these terms might simply suggest that potential and kinetic energy which has been residing in the time mean flow field is being transferred into a different flow configuration. However, these curves help us to identify the energetic signature of ring formation and, therefore, hypothesize the instabilities which may lead to it.

The question may be asked whether basin-averaged energetics are truly relevant in discussing the dynamical processes in the retroflection region. The basin energy budgets are obtained by integrating the model energy equations over the entire domain. If the flows were spatially homogeneous, basin budgets would adequately describe the energetics of every region in the domain. However, the flows under consideration are not homogeneous. One cannot tell from basin budgets the extent to which local energy budgets are different from the averaged budget. Harrison and Robinson (1978) showed that energy transfer averaged over a model domain may not be characteristic of any important subregion. BD showed, however, that most of K_M is localized in the boundary currents and K_E in the retroflection area (Fig. 3 of BD). In addition, time series of the total potential and kinetic energies and energy conversion terms show strong signals during ring formation. This, along with the fact that the retroflection region is the most energetic subregion of the domain, suggests that the energetics averaged over the whole basin give a reasonably good indication of events occurring in the retroflection area for these cases. Only in the low Rossby number case E1 does this not appear to entirely hold true.

As shown above, ring formation in E1 is quite different from that in E10 and E11. The retroflection in this experiment is highly variable, rings are formed almost continuously, and basin modes play a significant role. Further supporting this last assertion is the fact that the time series of the energy conversion terms $C(P, K_E)$ and $C(K_M, K_E)$ (Fig. 8a) are dominated by a 30-day signal, signature of the barotropic mode (5, 2) as defined in section 5a. In order to facilitate the identification of peaks in the energy conversion terms associated with ring formation, a low-pass filter at 40 days was applied to the two year time series (Fig. 8b). A small signal in $C(P, K_E)$ and intensification of the bottom layer anticyclone underneath the retroflection eddy preceding ring formation suggest the release of a

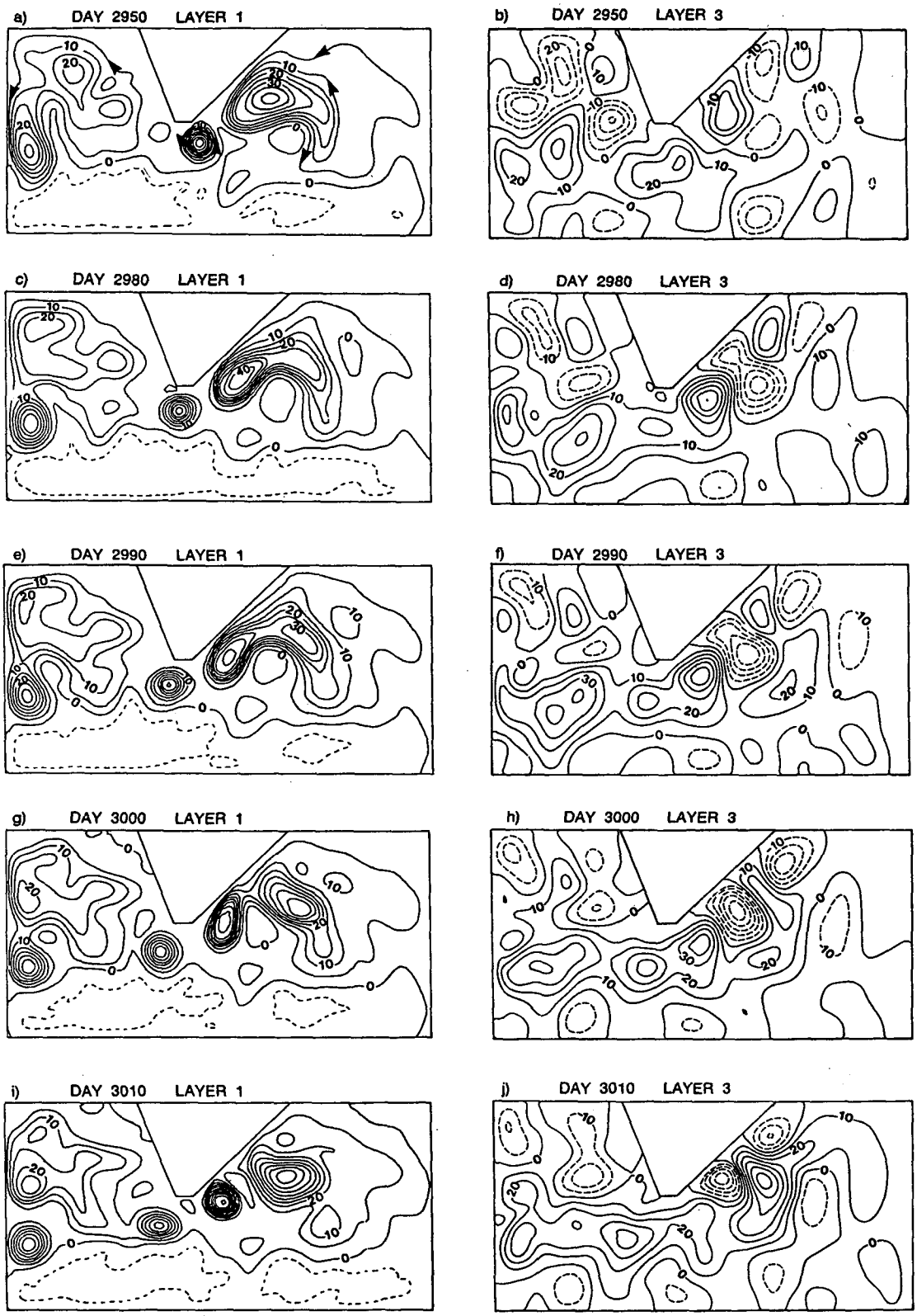

FIG. 7. As in Fig. 3 for E11, except the contour interval is 5 Sv for layer 1.

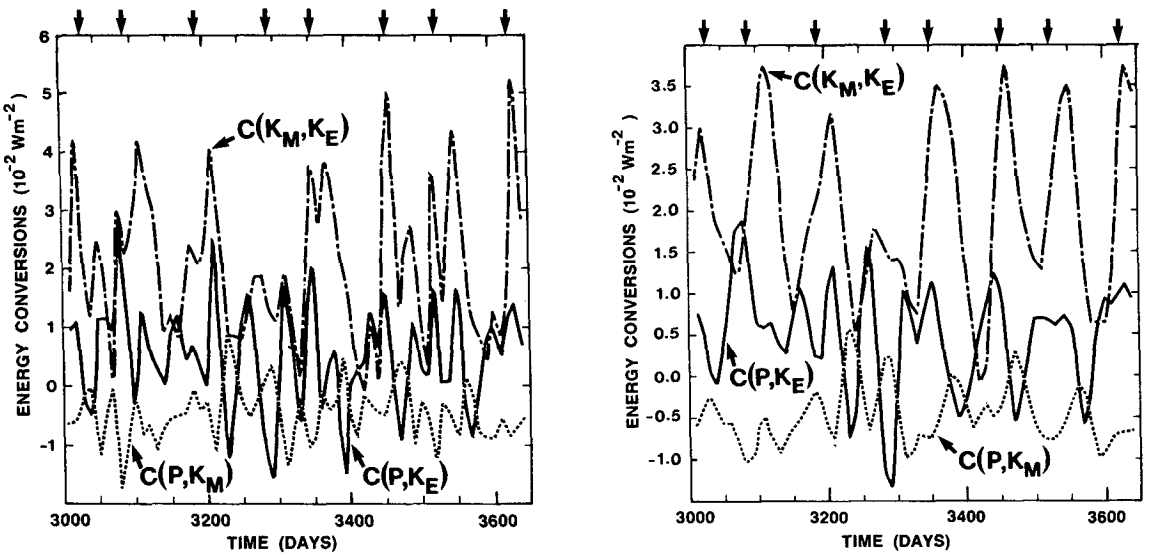

FIG. 8. Variations of the energy conversion terms with time in E1 (a) unfiltered, (b) 40 days lowpass filtered. Arrows indicate ring formation events.

weak baroclinic instability, as energy is transferred into the bottom layer. However, $C(P, K_E)$ is not always significant during ring formation, and from Fig. 8b we can conclude that ring formation is accompanied by significant peaks only in $C(K_M, K_E)$. These peaks reach their maxima shortly after a ring is formed. No signals are associated with ring formation, however, in time series of basin-averaged potential or kinetic energy (not shown). There exists some evidence, therefore, that both baroclinic and barotropic instability may play roles in E1 ring formation, but it is inconclusive.

In E10 and E11, ring formation events are separated by greater periods than in E1. It is therefore easier to identify signals in the energetics that may be associated with these events. In both experiments, significant peaks three to four times larger than in E1 appear during ring formation (Fig. 9 and Fig. 10). Both $C(K_M, K_E)$ and $C(P, K_E)$ in Fig. 9 reach a maximum just before ring cutoff. The bottom layer eddy field in the retroflection region has reached maximum intensity at that moment. Energy is injected downward as the flow reduces its vertical shear, as suggested by the peak in $C(P, K_E)$ at day 2875. This is characteristic of release of baroclinic instability. The latter is confirmed by a decrease in potential energy and an increase in kinetic energy from day 2860 to 2890 (Fig. 11), especially significant in the bottom layer where the kinetic energy triples in magnitude. In contrast, during the final pinching off [about day 2930 (Fig. 6c, d)], only a slightly positive baroclinic conversion is noted and the bottom layer is losing kinetic energy.

The two strong signals in Fig. 10 correspond to two events of ring formation in E11. The basic condition for the detachment in this experiment is amplification of the downstream meander in the return current, and whether this may be attributed to a particular instability is of interest. The dramatic growth of the cyclonic circulation in the third layer, illustrated in section 5c above, is suggestive that baroclinic instability is being released during ring formation. The latter is confirmed as in E10 by a decrease (increase) in potential energy (kinetic energy) during the period leading up to eddy detachment (Fig. 12). The bottom layer kinetic energy increase is not as strong as in E10. Before the meander begins to grow, the baroclinic conversion term is negative. Then, as the amplitude of the meander increases

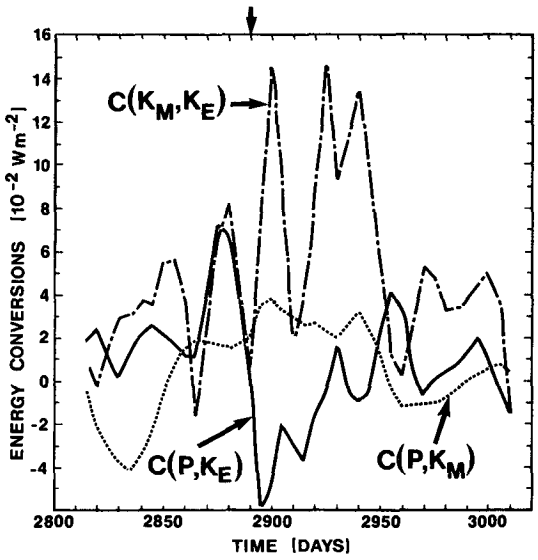

FIG. 9. As in Fig. 8a for E10.

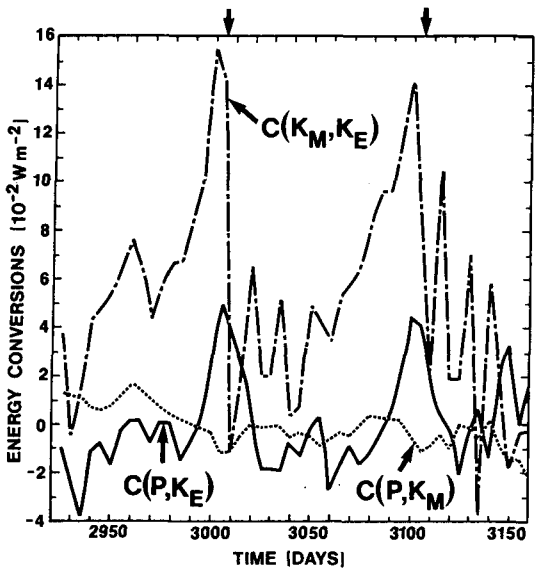

FIG. 10. As in Fig. 8a for E11.

and the bottom layer cyclonic circulation begins to intensify, $C(P, K_E)$ rises above zero and reaches a maximum just before ring cutoff. The barotropic conversion term reaches a maximum at the same time. That the maximum in $C(P, K_E)$ and the increase in bottom layer kinetic energy are smaller than in E10, both suggest that release of baroclinic instability plays a smaller role. This is supported by the fact that the retroflection region of E11 is not as vertically sheared as in E10, as shown in BC.

In E10 and E11, 1) both $C(K_M, K_E)$ and $C(P, K_E)$ peak just before ring formation and 2) ring formation is accompanied by a drop in total available potential energy and a gain in kinetic energy. It is, thus, suggested here that, in these two experiments, ring formation is associated with release of mixed barotropic–baroclinic instability.

6. Summary

The energetics of seven numerical experiments have been examined in some detail to help further understand the dynamics of Agulhas retroflection and ring formation in an idealized South Atlantic–Indian Ocean numerical model. We first reviewed the model characteristics and experimental design. The formulation of the energy conversion terms for the model was then presented and the basin-averaged eddy-mean energetics was examined. It was found, in particular, that experiments in which rings form exhibit considerably larger values of K_M to K_E transfer than those in which no rings form.

In addition, we investigated the ring formation process in a limited number of experiments, each of them very specific. Rings form in the model in the absence of any fluctuating forcing. The frequency of ring formation depends strongly on the choice of model parameters. With 40 km grid resolution and a rectangular Africa, inertia/baroclinicity in the overshooting Agulhas must be relatively weak in order for rings to form. As inertia increases, more fluid retroflects and fewer rings are formed. Halving the grid spacing better represents release of instabilities, especially baroclinic instability and to a lesser extent barotropic. This results in a few events of ring formation in a highly nonlinear case where there are none with 40 km grid spacing. A change to a more realistic geometry for Africa leads to ring formation along the coast, contrary to the previous

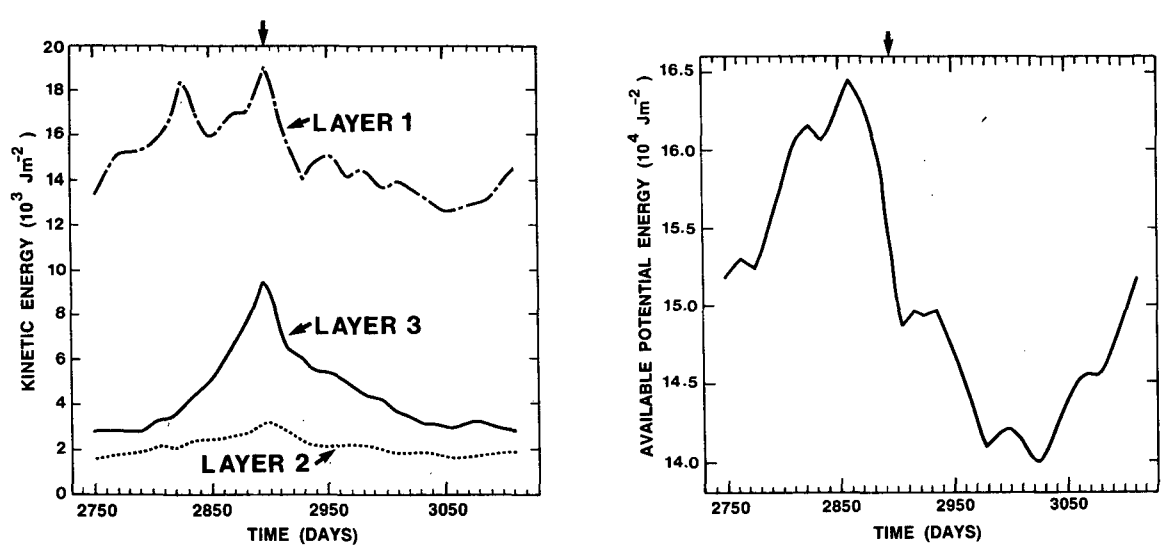

FIG. 11. Variations of the energies with time in E10 (a) kinetic energy, (b) available potential energy. Arrows indicate ring formation events.

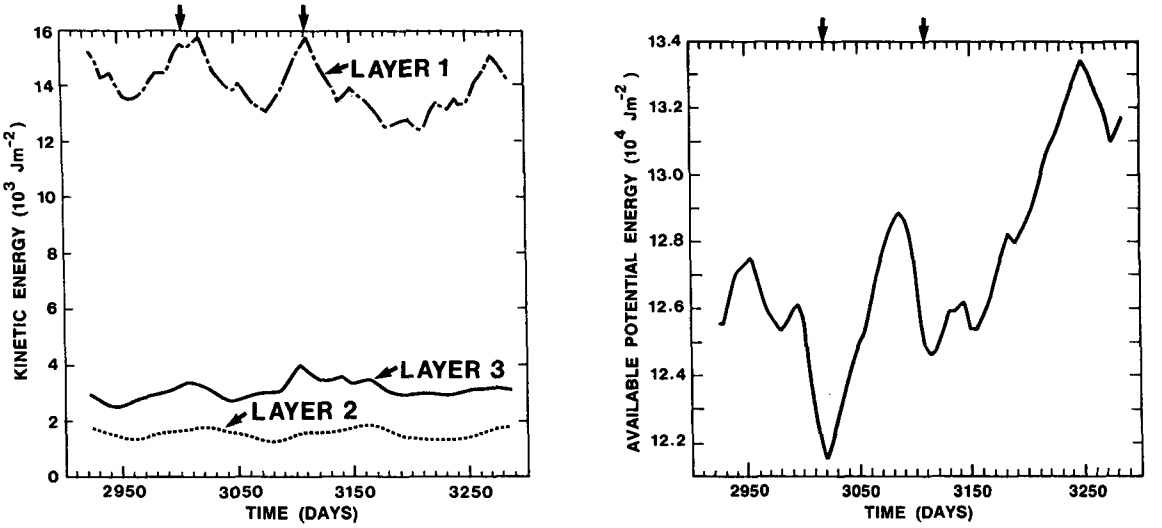

FIG. 12. As in Fig. 11 for E11.

rectangular cases, where rings form beyond the southern tip of Africa.

The ring formation process in the weakly nonlinear rectangular Africa case E1 is quite different from that in the highly nonlinear rectangular (E10) and triangular Africa (E11) cases. As soon as an already formed ring begins to escape into the Atlantic, the center of the retroflection moves south and a new ring begins to form. In addition, the regular ring formation in E1 is accompanied by a continual leakage of Indian Ocean water around the tip of Africa. This experiment exhibits an organized structure of elongated eddies in the bottom layer propagating east to west, representative of basin-mode resonance. The frequency of ring cutoff and the rings' subsequent westward motion are strongly related to those of the bottom layer features, suggesting a dynamical connection between them. Ring formation is accompanied by significant peaks in $C(K_M, K_E)$, but $C(P, K_E)$ is not always significant. In addition, no signals associated with ring formation appear in time series of basin-averaged potential or kinetic energy. Therefore, whether a form of instability (barotropic or baroclinic) plays a primary role in ring formation is unclear.

In E10, the ring is formed just southeast of the tip of Africa and in E11, the ring is formed near the southern tip along the coast. In each case, as the retroflection eddy becomes more intense, it draws more fluid into the downstream meander, the top of which accelerates toward the coast until the ring is cutoff from the main Agulhas. Only then does the ring start moving westward. Experiment E10 differs somewhat from E11 in that the ring, once formed, has more difficulty escaping into the Atlantic in the former. In both E10 and E11, ring formation events are separated by a greater period than in E1. It is therefore easier to identify signals in the energetics that may be associated with the events. Also in both, significant peaks in time series of domain-averaged energy conversions three to four times larger than in E1 appear during ring formation. Both $C(K_M, K_E)$ and $C(P, K_E)$ reach maxima just before ring cutoff. Release of baroclinic instability is confirmed by a decrease (increase) in basin-averaged potential (kinetic) energy. This is especially significant in E10 where the bottom layer kinetic energy triples in magnitude. It is therefore suggested here that, in these two experiments, ring formation is associated with release of mixed barotropic–baroclinic instability.

7. Discussion

In the comparison of the high resolution experiments with rectangular and triangular (more realistic) African geometry, it was suggested that the release of baroclinic instability associated with ring formation plays a smaller role in the latter. This is in accordance with one finding of Ou and de Ruijter (1986). In their study of the separation of an inertial boundary current on a β-plane using a one and one-half layer model, they found that, with an injection angle of 180° (corresponding to E10), the current path does not double back onto itself, contrary to the case with a 225° injection angle (corresponding to E11). Therefore, in E10, the eddy shedding can be viewed as due primarily to release of instability, which causes the downsteam meander to amplify until the retroflection eddy is cut off. In E11, since the inertial path tendency is already for the current to turn back onto itself, an instability associated with ring cutoff need not be as strong. That the instability must be particularly strong in E10 is supported by the relative infrequency of formation events. We should mention, on the other hand, that these comparisons must be viewed as qualitative since the Ou and de Ruijter model does not include coastal

friction, motion in more than one layer or temporal variability, as discussed in more detail in Part I (Boudra and Chassignet, 1988).

It is also interesting to draw analogies with other studies on ring formation, such as Gulf of Mexico and Gulf Stream rings. In their model study of the Gulf of Mexico Loop Current, Hurlburt and Thompson (1982) simulate eddy shedding. For their mixed instability case, they find 1) as we have here in E10 and E11, a rapid rise in the bottom layer kinetic energy when an eddy is shed, and 2) as in three of the above cases, an anticyclonic eddy in the bottom layer leading the westward advance of the Loop Current. In Ikeda's (1981) two-layer quasi-geostrophic study of meander growth and eddy detachment on an eastward flowing oceanic jet (application to the Gulf Stream), either a planetary or topographic β-effect is needed for an eddy to detach. The meanders are restricted to a spatially periodic case and grow larger because of a weak mixed barotropic–baroclinic instability. This is a similar regime in which rings form in our weakly nonlinear experiment (E1). However, when the meander is allowed to grow spatially, Ikeda and Apel (1981) show that eddies detach even in the absence of a β-effect. The large amplitude meanders shrink east–west and elongate north–south because of strong instabilities and nonlinear interactions with the other meanders and with the gyres, which further result in eddy detachment. This behavior is particularly characteristic of our high resolution, strongly nonlinear experiments.

We have made little attempt to compare our results with observation because our primary purpose has been to understand the dynamics of Agulhas ring formation in the model. In addition, there is still an enormous gap in complexity between the parameters of the model and the real characteristics of the South Atlantic–Indian Ocean: e.g., vertical stratification, basin size, coastal geometry, and bottom topography, to name a few. It is perhaps worth mentioning that rings formed in the model, especially in the 20-km resolution, high Rossby number experiments, exhibit many of the characteristics of observed Agulhas rings. Among these are ring diameters ($\sim$300 km), translation speed (4 to 8 cm s^{-1}), and circulating transport (30 to 50 Sv) (Olson and Evans, 1986, Gordon et al., 1987). Also, water of subpolar origin or that returning from the Atlantic at the southern boundary of the subtropical gyre is commonly found wedged between a newly formed Agulhas ring and the western edge of the main retroflection (Lutjeharms, 1984, personal communication). This is suggestive of a possible interaction between the Agulhas Return Current and this eastward drift, characteristic of many of the ring formation events in our high Rossby number experiments.

A fundamental aspect of ring formation clearly lacking from our model, but found in observations and the Ou and de Ruijter (1986) model, is the associated surfacing of the thermocline: that is, densely packed isopycnals outcrop along the edge of the retroflection loop and, thus, along the edge of the ring (e.g., see Gordon, 1985). In the Ou and de Ruijter model, the Agulhas' separation from the coast is achieved with the surfacing of the base of the top layer, which represents the thermocline since the lower layer is motionless. In our model, the chosen vertical stratification is not such that isopycnal outcropping occurs in the retroflection region. Especially since thermocline surfacing is characteristic of separation and ring formation associated with all the world's major western boundary currents, it seems that a next level of realism in our model's Agulhas retroflection and ring formation may be achieved through an enhancement of the vertical resolution. Such experimentation is in progress and will be reported shortly.

Acknowledgments. We wish to acknowledge helpful discussions with Drs. Lee Branscome, Don Olson and Claes Rooth. This work has been supported by the Office of Naval Research Contract N00014-85-C0020. Computations were performed using the Cray computers at the National Center for Atmospheric Research, which is sponsored by the National Science Foundation.

REFERENCES

Bleck, R., 1985: On the conversion between mean and eddy components of potential and kinetic energy in isentropic and isopycnic coordinates. *Dyn. Atmos. Oceans*, **9**, 17–37.

——, and D. B. Boudra, 1981: Initial testing of a numerical ocean circulation model using a Hybrid (quasi-Isopycnic) vertical coordinate. *J. Phy. Oceanogr.*, **11**, 755–770.

Bleck, R., and D. B. Boudra, 1986: Wind-driven spin-up in eddy-resolving ocean models formulated in isobaric and isopycnic coordinates. *J. Geophys. Res.*, **91**(C6), 7611–7621.

Boudra, D. B., and W. de Ruijter, 1986: The wind-driven circulation in the South Atlantic-Indian Ocean. II. Experiments using a multi-layer numerical model. *Deep-Sea Res.*, **33**, 447–482.

——, and E.P. Chassignet, 1988: Dynamics of Agulhas retroflection and ring formation in a numerical model. Part I. The vorticity balance. *J. Phys. Oceanogr.*, (in press.)

De Ruijter, W., and D. B. Boudra, 1985: The wind-driven circulation in the South Atlantic-Indian Ocean. I. Numerical experiments in a one-layer model. *Deep-Sea Res.*, **32**, 557–574.

Duncan, C. P., 1968: An eddy in the subtropical convergence southwest of South Africa. *J. Geophys. Res.*, **73**, 531–534.

Dutton, J. A., 1976: *The Ceaseless Wind.* McGraw Hill, 579 pp.

Gordon, A. L., 1985: Indian–Atlantic transfer of thermocline water at the Agulhas Retroflection. *Science*, **227**, 1030–1033.

——, 1986: Interocean exchange of thermocline water. *J. Geophys. Res.*, **91**, 5037–5046.

——, J. R. E. Lutjeharms and M. L. Gründlingh, 1987: Stratification and circulation at the Agulhas retroflection. *Deep-Sea Res.*, **34**, 565–599.

Harris, T. F. W., R. Legeckis and D. van Foreest, 1978: Satellite infra-red images of the Agulhas Current System. *Deep-Sea Res.*, **25**, 543–548.

Harrison, D. E., and A. R. Robinson, 1978: Energy analysis of open regions of turbulent flows—mean eddy energetics of a numerical ocean circulation experiment. *Dyn. Atmos. Oceans*, **2**, 185–211.

Holland, W. R., 1978: The role of mesoscale eddies in the general circulation of the ocean—numerical experiments using a wind-driven quasi-geostrphic model. *J. Phys. Oceanogr.*, **8**, 363–392.

Hulburt, H. E., and J. D. Thompson, 1980: A numerical study of

Loop Current intrusions and eddy shedding. *J. Phys. Oceanogr.*, **10,** 1611–1651.

——, and ———, 1982: The dynamics of the Loop Current and shed eddies in a numerical model of the Gulf of Mexico. *Hydrodynamics of Semi-enclosed Seas,* J. C. J. Nihoul Ed., Elsevier, 243–298.

Ikeda M., 1981: Meanders and detached eddies of a strong eastward-flowing jet using a two-layer quasi-geostrophic model. *J. Phys. Oceanogr.*, **11,** 526–540.

——, and J. R. Apel, 1981: Mesoscale eddies detached from spatially growing meanders in an eastward-flowing oceanic jet using a two-layer quasi-geostrophic model. *J. Phys. Oceanogr.*, **11,** 1638–1661.

Lamb, H., 1932. *Hydrodynamics.* 6th ed. Cambridge University Press, 738 pp.

Longuet-Higgins, M.S., 1964: Planetary waves on a rotating sphere. *Proc. Roy. Soc.,* **279,** 446–473.

Lutjeharms, J. R. E., 1981: Spatial scales and intensities of circulation of the ocean areas adjacent to South Africa. *Deep-Sea Res.*, **28A,** 1289–302.

——, and A. L. Gordon, 1987: Shedding of an Agulhas ring observed at sea. *Nature,* **325,** 138–140.

——, and R.C. van Ballegooyen, 1987: Retroflection of the Agulhas Current. *J. Phys. Oceanogr.,* (submitted.)

Miller, A. J., W.R. Holland and M.C. Hendershott, 1987: Open-ocean response and normal modes excitation in an eddy-resolving general circulation model. *Geophys. Astrophys. Fluid Dyn.*, **37,** 253–278.

Nof, D., 1983: On the migration of isolated eddies with application to Gulf Stream rings. *J. Mar. Res.*, **41,** 399–425.

Olson, D. B., and R. H. Evans, 1986: Rings of the Agulhas. *Deep-Sea Res.*, **33,** 27–42.

Ou, H. W., and W. de Ruijter, 1986: Separation of an inertial boundary current from a irregular coastline. *J. Phys. Oceanogr.*, **16,** 280–289.

Pearce, A. F., and M. L. Gründlingh, 1982: Is there a seasonal variation in the Agulhas current? *J. Mar. Res.*, **40,** 177–184.

Pedlosky, J., 1965: A study of the time-dependent ocean circulation. *J. Atmos. Sci.*, **22,** 267–272.

Stommel, H., 1980: Asymmetry of interoceanic fresh-water and heat fluxes. *Proc. Natl. Acad. Sci. USA,* **77,** 2377–2381.